Mitochondrial Metabolism in Developing Embryos of *Brassica napus*

Jörg Schwender, Yair Shachar-Hill and John Ohlrogge

Supplemental Text

1. Metabolic Network

1.1 Network definition. A network of central metabolism containing the reactions of glycolysis, oxidative pentosephosphate pathway (OPPP), RubisCO, the tricarboxylic acid (TCA) cycle and fatty acid synthesis was defined as shown in Fig. S1. The key features are the same as reported in Schwender et al. (2003) for *B. napus* embryos with the addition of the reactions of the TCA cycle as well as the RubisCO and phosphoribulokinase reactions. The core TCA cycle enzymes as well as mitochondrial malic enzyme were considered (Fig. S1). Reactions specific for the glyoxylate cycle were not considered because significant activity of the key enzymes have not been detected during the main phase of storage accumulation (Chia et al., 2005). In fact, if mitochondrial isocitrate lyase together with malate synthase were added to the model, flux parameter fitting consistently assigned very small fluxes to these reactions and the quality of the fit was not increased by their inclusion (data not shown). In relation to the TCA cycle, cytosolic ATP:citrate lyase was considered to produce cytosolic acetyl-CoA for the cytosolic elongation of fatty acids as described before (Schwender and Ohlrogge, 2002). Also the RubisCO reaction was added as this enzyme is known to be abundant and active *in vivo* in developing *B. napus* embryos (Ruuska et al., 2004) and has been shown to carry flux *in vivo* (Schwender et al., 2004). The network is shown compartmentalized only in reactions downstream of phosphoenol pyruvate because labeling experiments indicated a high exchange of several glycolytic intermediates between cytosol and plastid (Schwender et al., 2003). Therefore, reactions upstream of PEP are modeled without considering separation into cytosolic and plastidic compartments. For example, *vG6PDH* summarizes the flux through both plastidic and cytosolic *G6PDH*.

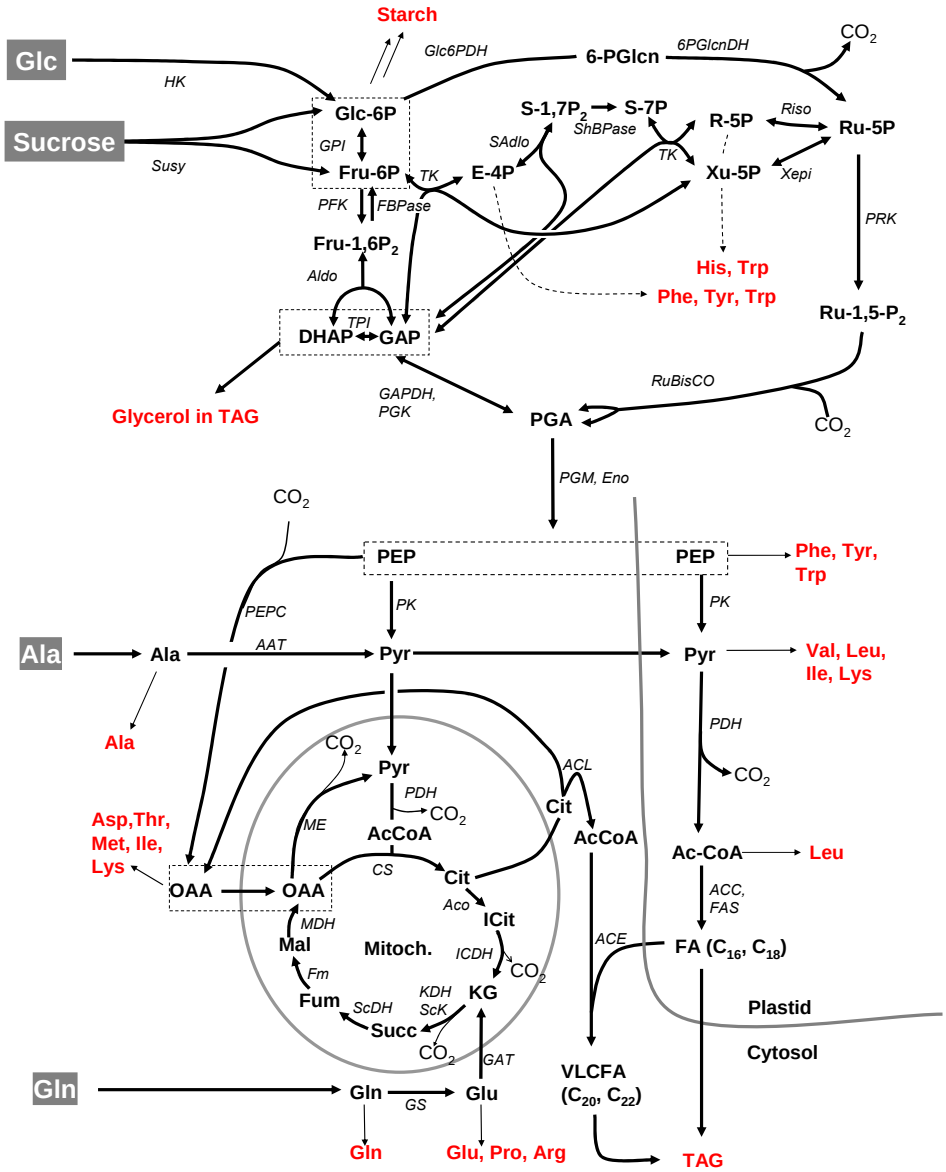

Fig. S1 Metabolic network, showing the main reactions of central metabolism known to be present in developing, oil accumulating *B. napus* embryos. The carbon sources provided to embryo cultures are shown as well as all the major biosynthetic products stored in the seeds (red). Dashed boxes designate central metabolites that were assumed to equilibrate isotopically by fast interconversion based on experimental data (see section 6) **Enzymes**: ACC: acetyl-CoA carboxylase; ACE: acyl-CoA elongase; ACL: ATP:citrate lyase; Aco: aconitase; Aldo: fructose 1,6-bisphosphate aldolase; AAT: alanine transaminase; CS: citrate synthase; Eno: enolase; FBPase: fructose 1,6 bisphosphatase; FAS: fatty acid synthase; Fm: fumarase; GAPDH: glyceraldehyde 3-phosphate dehydrogenase; GAT: glutamyl aminotransferase; Glc6PDH: glucose 6-phosphate dehydrogenase; GPI: glucose 6-phosphate isomerase; GS: glutamate synthase; HK: hexokinase; ICDH: isocitrate dehydrogenase; KDH: ketoglutarate dehydrogenase; MDH: malate dehydrogenase; ME malic enzyme; PDH: pyruvate dehydrogenase; PEPC: phosphoenol pyruvate carboxylase; PFK: phospho fructokinase; PGM: phosphoglycerate mutase; PGK: phosphoglycerate kinase; PK: pyruvate kinase; PRK: phosphoribulokinase; 6PGlcnDH: 6-phosphogluconate dehydrogenase; Riso: ribose 5-phosphate isomerase; RuBisCO: ribulose 1,5-bisphosphate carboxylase/oxygenase; SAldo: sedoheptulose 1,7-bisphosphate aldolase; ScDH: succinate dehydrogenase; ScK: succinate kinase; ShBPase: sedoheptulose bisphosphatase; SuSy: sucrose synthase; TK: transketolase; Xepi: xylulose 5-phosphate epimerase; TPI: triose phosphate isomerase. **Metabolites**: 6-PGlcn: 6-phosphogluconate; Cit: citrate; DHAP: dihydroxy acetone phosphate; E-4P: erythrose 4-phosphate; Fru-1,6P2: fructose 1,6-bisphosphate; Fru-6P: fructose 6-phosphate; Fum: fumarate; GAP: glyceraldehyde 3-phosphate; Glc-6P: glucose 6-phosphate; ICit: isocitrate; KG: ketoglutarate; Mal: malate; OAA: oxaloacetate; PEP: phosphoenol pyruvate; PGA: 3-phosphoglycerate; Pyr: pyruvate; R-5P: ribose 5-phosphate; Ru-1,5P2: ribulose 1,5-bisphosphate; Ru-5P: ribulose 5-phosphate; Sh-1,7P2: sedoheptulose 1,7-bisphosphate; Sh-7P: sedoheptulose 7-phosphate; Succ: succinate; TAG: triacyl glycerol; VLCFA: very long chain fatty acids; Xu-5P: xylulose 5-phosphate;

1.2 Isotopic imprinting in proteinogenic amino acids and fatty acids.

In a retro-biosynthetic approach the labeling in central metabolites such as phosphoenol pyruvate, pyruvate or oxaloacetate can be derived from the labeling of their products Phe, Val and Asp, respectively (Szypersky 1998). The particular amino-acid–precursor relations are summarized in Table S4 and Fig. S2. Instead of extracting and analyzing labeling in low abundance intermediates, labeling in storage proteins and oil was measured and analyzed by GC/MS methods as described before (Schwender and Ohlrogge 2002, Schwender et al., 2003). The fractional ^{13}C-enrichment in protein amino acids and fatty acids was interpreted according to the biosynthetic relationship between precursors and their products accumulating in biomass (Fig. S2).

1.3 Subcellular localization of amino acid synthesis

The following assumptions were made about the subcellular localization of amino acid syntheses: The biosyntheses of His, Val, Leu, and Ile are exclusively plastidic (Ohta et al., 2000; Singh et al., 1999). Their labeling represents that in plastidic pentose phosphate (His), pyruvate (Val) and aspartate (Leu and Ile). Also the key enzymes in aromatic amino acid (Phe, Tyr, Trp) biosynthesis are known to be plastid-localized. In the absence of photorespiration in *B. napus* embryos (Schwender et al. 2002, Goffman et al., 2004), serine is formed from PGA by the plastidic phosphorylated serine biosynthetic pathway (Ho et al., 1999). However, a signature of the interconversion of Ser and Gly by serine hydroxymethyl transferase can be observed in the labeling pattern of Ser (data not shown) making Ser unsuitable as a reporter for labeling in PGA.

Protein amino acids were assumed to be derived from their cytosolic pools independent from the subcellular compartment of their biosynthesis. This is because the protein analyzed consists almost entirely of storage proteins which are synthesized in the cytosol, presumably from amino acid tRNAs formed in the cytosol.

Aspartate and Glutamate can be derived from oxaloacetate and α-ketoglutarate, respectively, in different compartments by transamination (Schultz and Coruzzi, 1995; Wilkie and Warren, 1998). Assuming abundant cytosolic aminotransferase activities, one can assume that protein-bound Asp and Glu represent cytosolic OAA and KG, respectively.

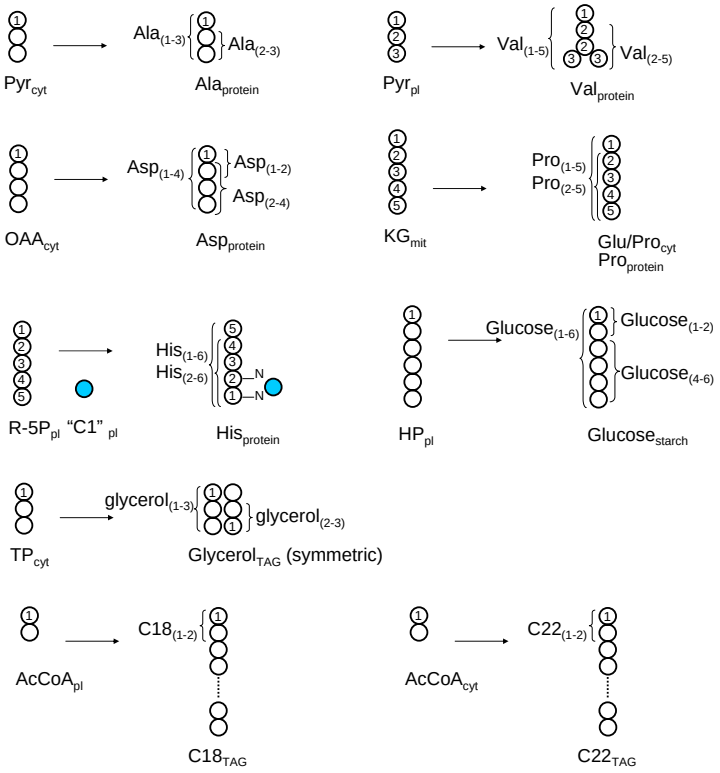

Fig. S2 Relationships between particular carbon atoms of central metabolites and those of monomers in biomass compounds. The numbers in the carbon atoms (circles) denote the carbon positions of the precursors while the indices (subscripts) defining the MS fragments are the carbon positions of the monomers. The carbon transitions of amino acid biosynthesis can be derived from general biochemistry textbooks.

Since protein is acid-hydrolyzed prior to amino acid analysis Gln is deaminated to Glu. Therefore Glu in the hydrolysate is derived from both Gln and Glu of the protein. Therefore, the label observed in protein-derived Glu was not used for modeling. Instead Pro, which is directly biosynthetically derived from Glu, was used and assumed to represent the label in cytosolic Glu. In several experiments, when labeled free amino acids were extracted and analyzed, the labeling pattern in Glu and Pro were always found to be identical, showing labeling signatures related to mitochondrial ketoglutarate (data not shown).

1.4 Subcellular compartmentation of Acetyl-CoA.

In plants, fatty acid synthesis is predominantly localized in plastids (Ohlrogge et al., 1979, Dennis, 1989). Plastidic fatty acid synthesis produces C16 and C18 fatty acids, whereas the elongation of C18:1 by a cytosolic fatty acid elongation system produces C20 and C22 fatty acids (Domergue et al., 1999; Whitfield et al., 1993). Thus, labeling in the carboxyl-terminal acetate units of C18 and C22 fatty acids represent plastidic and cytosolic acetyl-CoA pools, respectively (Schwender and Ohlrogge, 2002). Terminal acetate units of C18 and C22 methyl esters are monitored in the Fragment m/z 74 (McLafferty fragment) as described in Schwender et al. (2003).

2. Isotopomer Model

A steady state metabolic model was used in this study with the topology of the metabolic network defined by the stoichiometries and the carbon transitions of the biochemical reactions. The biomass composition of the embryos defines the fluxes of metabolites into biomass. Given the ^{13}C-labeling of substrates and values for the fluxes, the model simulates all MS measurements. The model described here is able to simultaneously simulate MS measurements for three different labeled substrates ([1,2-$^{13}C_2$]glucose/[U-$^{13}C_6$]glucose, [U-$^{13}C_5$]Gln and [U-$^{13}C_3$]Ala, respectively).

2.1 Steady state isotopomer model. Isotopomer balancing and flux parameter fitting were performed using the software package *13CFLUX* (obtained from Prof. Dr. W. Wiechert, Department of Simulation, University of Siegen, Germany) on a X86 compatible computer as described by Wiechert and co-workers (Wiechert et al. 2001, and refs cited therein). The software was run under RedHat Linux. *13CFLUX* allows the implementation of metabolic network models by allowing the user to define the label input, the network stoichiometry, the carbon transitions and definitions of measured labeling patterns (NMR and MS data). Biochemical conversions are defined as net and exchange fluxes (V_{net}, V_{Xch}) which are related to the conventional forward and reverse fluxes according to Wiechert and DeGraaf, 1997:

$V_{forward} = V_{net} + V_{XCH}$
$V_{backward} = V_{net} - V_{XCH}$

In cases where a reaction is assumed to be irreversible, the respective exchange flux is set to zero and the value of the flux is constrained to being positive.

With *13CFLUX* it is possible to fit simulated labeling patterns to experimental data (Non-linear least-squares fitting approach). Several evolutionary algorithms of the software-package were used to find flux values that most likely represent a global optimum fit (section 4). Statistical tools in *13CFLUX* allow the errors in the fluxes to be derived based on linearized statistical analysis (see section 5).

2.2 Metabolic model combining three labeling experiments. The central metabolic network for developing *B. napus* embryos (Fig. S1) containing the reactions of glycolysis, oxidative and non-oxidative pentosephosphate pathway (PPP), RubisCO, the tricarboxylic acid (TCA) cycle and fatty acid synthesis was implemented by defining stoichiometry and carbon transitions, which are taken from standard biochemistry textbooks. An overview over all metabolic pools and reactions implemented in the model is given in Fig. S3. Essential parts of the *13CFLUX* model files for embryos are shown in Table S10.

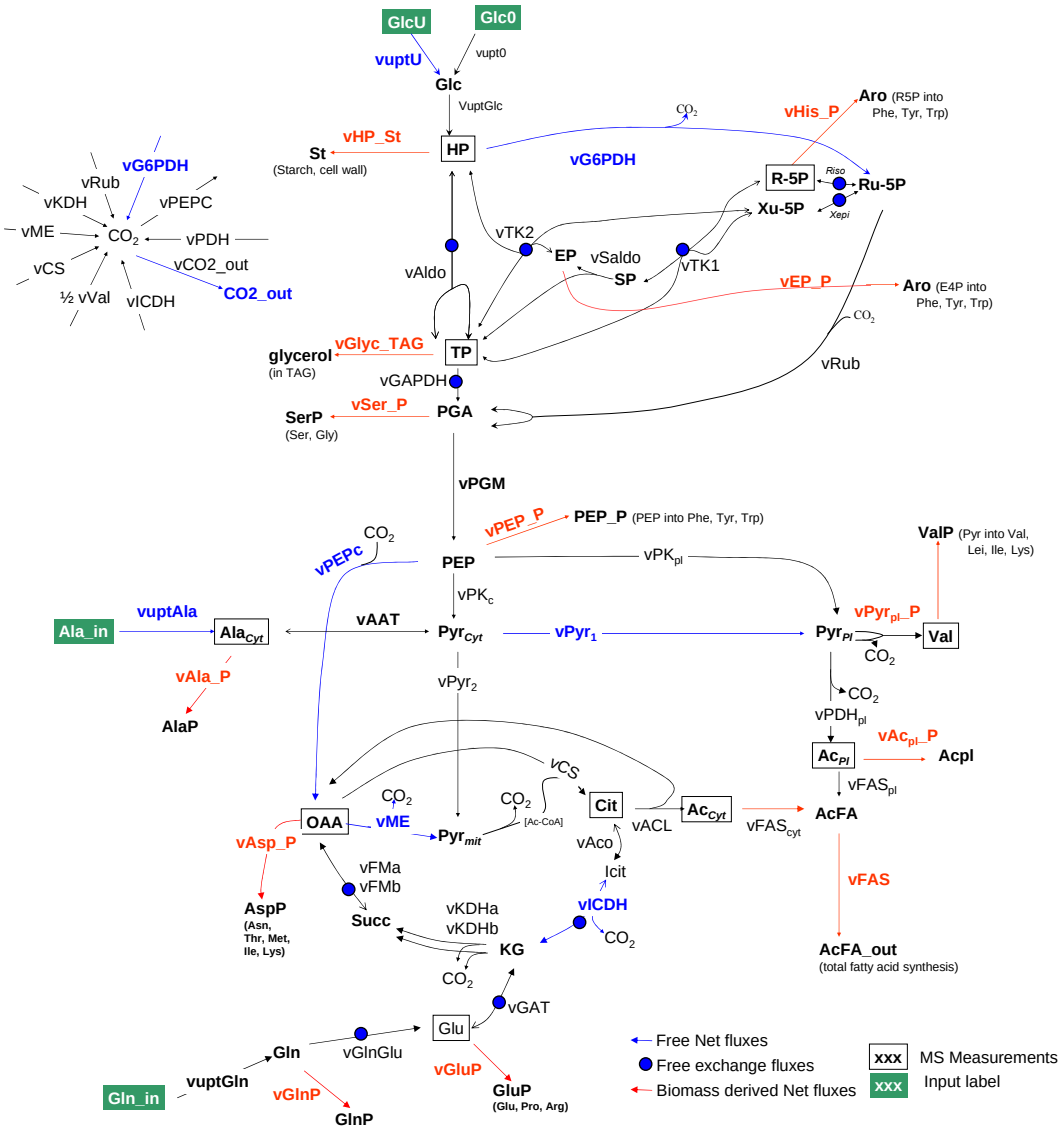

Fig. S3: Model network as derived from Fig. S1 and implemented in *13CFLUX (See Table S10)*. The figure shows the reactions with flux and metabolite names used in the model file. Input metabolites are shown in green. Free variable fluxes are in blue. Fluxes into biomass synthesis (biomass constraints) are in red. Double headed arrows designate reactions that are modeled reversibly. Ac: Acetyl-CoA; AcFA: acetate units in fatty acids; Cit: citrate; ICit: isocitrate; EP: erythorse 4-phosphate; HP: hexose phosphates; PDH: pyruvate dehydrogenase; PEP:phosphor enolpyruvate; PGA: phosphoglycerate; Pyr: pyruvate; PK: pyruvate kinase; R-5P: ribose 5-phosphate; Ru-5P: ribulose 5-phosphate; SP: sedoheptulose 7-phosphate; TP: triose phosphates; Xu-5P: xylulose 5-phosphate.

In order to simultaneously predict labeling measurements for experiments with different labeled substrates in one model the *13CFLUX* model file contains a repetition of all reaction equations of the basic flux model shown in Fig. S3. The parallel sub model-networks were distinguished by their flux names (see Table S10). In each sub-network a flux name (<*fluxname*>) was designated according to "v<*fluxname*>", "v2<*fluxname*>" or "v3<*fluxname*>" and metabolite names accordingly as "m1<*metabolitename*>", "m2<*metabolitename*>" and "m3<*metabolitename*>". Also, different definitions for label input metabolites in the three sub-networks were defined according to Fig. S4A.

The sub models were connected by adding linear flux dependencies (section "EQUALITIES" in the *13CFLUX* model file) in a way that defines all the fluxes of the second and the third sub-models to equal the corresponding fluxes in the first one (Fluxes defined as dependent). In this way, by definition of the free fluxes in the first sub-model, the complete model simulates the isotopomer distributions of all three labeling experiments dependent on the flux distribution in the model shown in Fig. S3. This allows the optimization of flux parameters to simultaneously fit the labeling data of all three experiments using different labeled precursors.

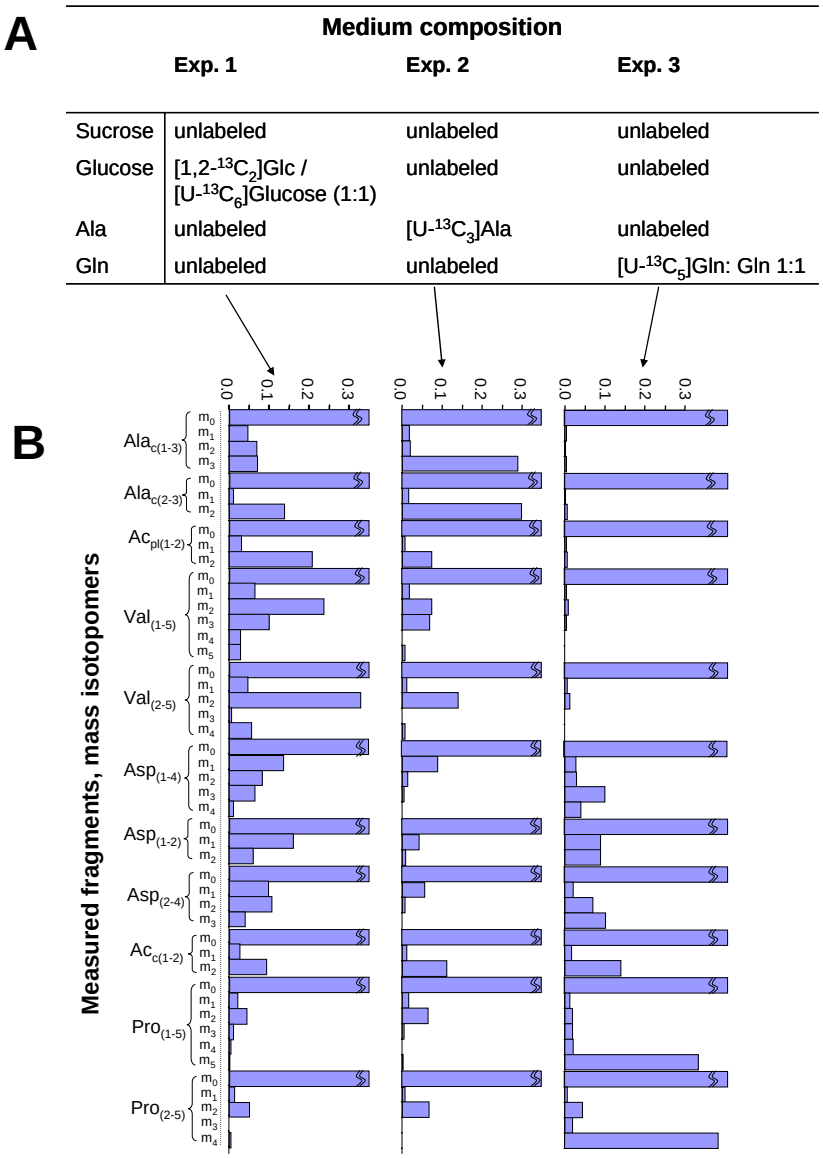

Fig. S4: Combination of three labeling experiments in flux parameter fitting and statistical analysis (see also table S6). A) Medium composition in the three labeling experiments. B) Fractional ^{13}C-enrichments (mass isotopomer abundance) in 11 selected fragments resulting from the three experiments. As shown, each experiment results in a different labeling pattern for most fragments.

3. Measurements

The flux estimation was constrained by the ^{13}C-labeling pattern in metabolites and by the biomass composition which together allow fluxes of central metabolism and seed storage product synthesis to be derived. In addition ^{15}N labeling data were used to derive the extent of reversibility of transaminase reactions as described below under sections 4.1 and 6.3.

3.1 Biomass derived fluxes. Fluxes of metabolites (e.g. pyruvate or oxaloacetate) out of central metabolism into oil, storage protein and carbohydrate polymers (Fig. S3, red arrows) are derived from the biomass composition. For embryos grown in culture, oil, protein, starch, and cell wall polymers were considered as biomass components (Table S1). From the fatty acid composition of seed oil (Table S3) and the amino acid composition in storage protein (Table S2) the quantities of monomers (proteinogenic amino acids as well as glycerol and cytosolic and plastidic acetyl units, respectively) can be derived. The amount of hexose-phosphate used for glucose polymers (starch and cell walls) comes directly from the molar weight of glucose in a glucose polymer ((180 – 18) g/mol). With the stoichiometries of the biosyntheses of the monomers, the biosynthetic demands on the central metabolites (like pyruvate, OAA) can be derived. Finally, by considering the growth rate of the embryos an absolute flux rate "[$\mu mol\ h^{-1}\ gDW^{-1}$]" of intermediates into biomass synthesis can be given as shown in table 1 of the main text.

3.2 Label Measurements. As described in the main text, the measured mass isotopomer fractions are averages from three GC/MS runs and were corrected for the contributions of natural abundance of isotopes of C, H, N, O, S and Si. For a given C_n-fragment in the mass spectrum of a labeled compound the corrected mass isotopomer fractions are [m_0, m_1, … m_n] with the sum of all mass isotopomers equal to 1 or 100 %. In the following the resulting corrected mass isotopomer fractions are called "Label Measurements". The label measurements were defined in the *13CFLUX* model files as "cumomer fractions" (Wiechert et al., 1999).

For each of the three labeling experiments more than 150 mass isotopomer fractions were determined by GC/MS analysis. Out of these data in each experiment 47 label measurements were added into the flux model (see Fig. S4, Table S6) (TBDMS derivatives of Asp, Pro, Ala, Val; C18 and C22 fatty acid methyl esters). Not used in the flux model were measurements of amino acids which have the same precursor (e.g. Thr is derived from Asp and always showed the same labeling pattern as Asp). In the case of the [1,2-$^{13}C_2$]glucose / [U-$^{13}C_6$]glucose labeling, MS measurements of glucose-methoxime pentaacetate, TBDMS-histidine and the glycerol-TFA were also considered - being derived from starch, protein and triacylglycerols, respectively (Table S7). The labeling in Ribose-5P was derived from the labeling in histidine which is composed of a ribosyl part and N^{10}-Formyl-THF derived carbon (C-6 of His; Fig. S3). Assuming that C-2 of Gly represents labeling in N^{10}-formyl-THF, the labeling in Riblose-5P ($RP_{(1-5)}$) was derived from the labeling in His ($His_{(1-6)}$) and Gly ($Gly_{(2)}$) by linear regression according to:

$$\begin{bmatrix} m_0 & 0 & 0 & 0 & 0 & 0 \\ m_1 & m_0 & 0 & 0 & 0 & 0 \\ 0 & m_1 & m_0 & 0 & 0 & 0 \\ 0 & 0 & m_1 & m_0 & 0 & 0 \\ 0 & 0 & 0 & m_1 & m_0 & 0 \\ 0 & 0 & 0 & 0 & m_1 & m_0 \\ 0 & 0 & 0 & 0 & 0 & m_1 \end{bmatrix} \times \begin{bmatrix} r_0 \\ r_1 \\ r_2 \\ r_3 \\ r_4 \\ r_5 \end{bmatrix} = \begin{bmatrix} h_0 \\ h_1 \\ h_2 \\ h_3 \\ h_4 \\ h_5 \\ h_6 \end{bmatrix}$$

Mass isotopomer mapping matrix $RP_{(1-5)}$ $His_{(1-6)}$
Derived from $Gly_{(2)}$.

(In the mapping matrix m_0 and m_1 describe the fractional ^{13}C-label in C2 of glycine, as derived by MS measurements from TBDS-Gly ($Gly_{(2)}$). Vector $RP_{(1-5)}$ [r_0 … r_5]: fractional ^{13}C-label in $RP_{(1-5)}$; Vector $His_{(1-6)}$ [h_0 … h_6]: fractional ^{13}C-label in $His_{(1-6)}$ as derived from MS measurements of TBDS-His.)

4. Flux parameter fitting

4.1 Least squares fitting procedure: In order to find flux values in the model network that best explain the biomass derived fluxes and fractional labeling data, the simulated MS measurements calculated by the model are compared to the experimental data. The problem of finding the best fit is solved by a non-linear least-squares fitting approach. The procedure of flux parameter fitting is summarized in Fig. S5. The sum of squared differences between model predictions and experimental measurements is minimized by variation in the free flux parameters. Due to the non-linearities in the isotopomer model there is no guarantee that an identified minimum of least squares represents the global minimum. Therefore, as is general practice in literature on ^{13}C-flux analysis the flux values obtained should be referred to as the "best estimates".

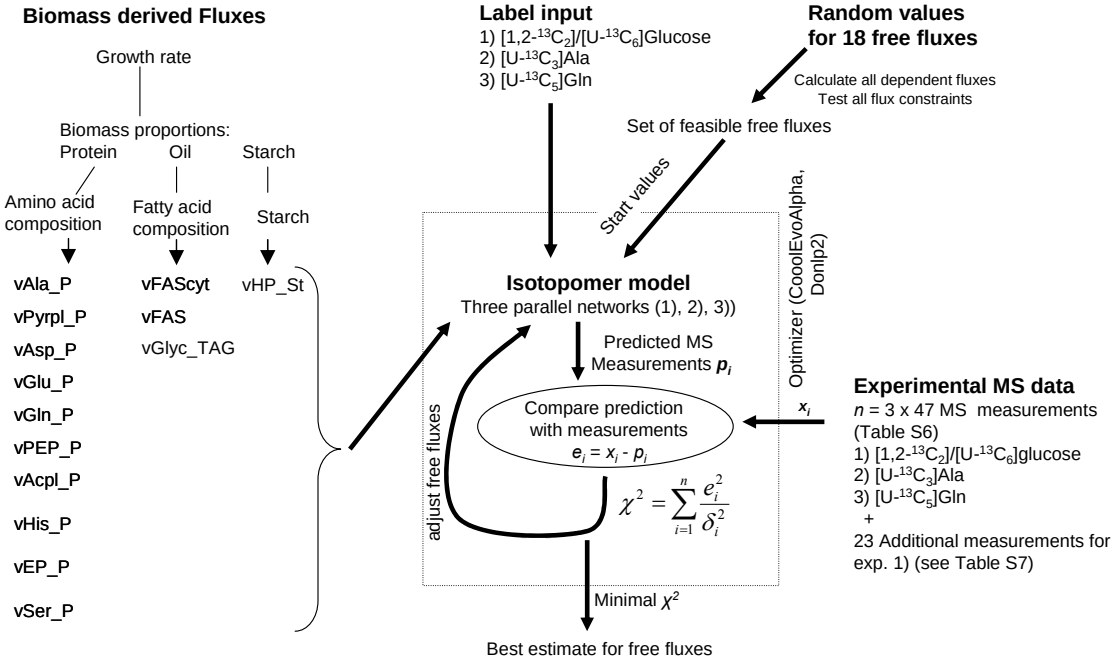

Fig. S5: The procedure used for flux parameter fitting. Details see text. For flux names compare Fig. S3. e_i : residuals; x_i : measurements; p_i: simulated values; δ_i : standard deviation of measurement i.

4.2 Computational flux fitting. For flux optimization, the program *CooolEvoAlpha*, an evolutionary algorithm from the *13CFLUX* software package as well as the *13CFLUX* implementation of *Donlp2* (sequential quadratic programming algorithm by Peter Spellucci, Technische Universität Darmstadt, Germany) were used. Both algorithms gave the same general results while Donlp2 needs considerably less computing time. During optimization, the sum of errors (squared differences between model predictions and experimental measurements, weighted by SD^2) is minimized (Fig. S5). The algorithms continue variation of the flux parameters until the sum of errors cannot be further diminished. Wide-ranging tests have shown that whether the flux parameter fitting is performed with the original SD derived from MS measurements or by assuming one

value for all standard deviations (see section 5), the resulting best estimate of flux is consistently reproduced and is virtually the same.

Flux optimization was repeated with random generated flux parameter sets as starting values. Only those flux sets were used which are feasible within the stoichiometric constraints in the flux parameter space of the network.

Initially, analysis of 30 optimized flux sets showed that the algorithm consistently converged to very similar low residuals with one solution for most free net fluxes, while *vPyr1* (see Fig. S3) was fixed with some variation. Within this variability *vPyr1* is negatively correlated with the exchange flux $vAAT_{XCH}$, which describes the interconversion rate of Pyr_{cyt} and Ala_{cyt} (Alanine amino transaminase). This means the model explains the MS data equally well with different combinations $vAAT_{XCH}$ and *vPyr1*. This suggests that the part of the network connecting cytosolic alanine and plastidic pyruvate, in particular the exchange flux $vAAT_{XCH}$, cannot be resolved by ^{13}C-data alone. This missing information is contained in data resulting from labeling with ^{15}N-Ala or ^{15}N-Gln (table S7a) because reversible transaminase activity exchanges amino groups between amino acids. Assuming that the α-nitrogen of Ala is derived from alanine which is derived from the medium and labeled at 99 % ^{15}N, as well as derived by transamination from ^{14}N-Glu, the steady state equations for the α-nitrogen of Ala_c can be derived (Fig. 1 in main text):

1) Mass balance of ^{15}N-label:

$$\left(vAla_P + vAAT_{NET} + vAAT_{XCH}\right)\times\left[\%^{15}N(Ala_c)\right] = vuptAla\times\left[\%^{15}N(Ala_{medium})\right] + vAAT_{XCH}\times\left[\%^{15}N(Glu_{protein})\right]$$

2) The ^{15}N enrichment in $Ala_{protein}$ equals the enrichment in Ala_c. As well the label in $Pro_{protein}$ represents Glu.

3) steady state

$$\frac{dAla_c}{dt} = vuptAla + vAAT_{XCH} = vAla_{Prot} + vAAT_{NET} + vAAT_{XCH} = 0$$

From 1), 2) and 3) we obtain:

$$\frac{vAAT_{XCH}}{vupt_{Ala}} = \frac{\left[\%^{15}N(Ala_{medium})\right] - \left[\%^{15}N(Ala_{protein})\right]}{\left[\%^{15}N(Ala_{protein})\right] - \left[\%^{15}N(Pro_{protein})\right]}$$

Using these equations and the ^{15}N-measurements (table S7a), the value for $vAAT_{XCH}$ was constrained to 25.8 ± 11.4 times the input flux of alanine (*vuptAla*). In this range of values, Ala_C and Pyr_C will always be near isotopic equilibrium.

As a result of this consideration the exchange flux $vAAT_{XCH}$ was fixed to be 25.8 times the influx of Ala (*vuptAla*).

After the adjustment for $vAAT_{XCH}$ based on ^{15}N-labeling results the optimizer algorithm was started 100 times with random start values for the free fluxes (Fig. S3) and the evolutionary algorithm converged consistently to one solution with lowest "residuum" (residual sum of deviations, see figure S5) for the free net fluxes, suggesting a global optimum. The best flux estimates are shown in table S8 and table 1 in the main text.

If the model predictions and the MS measurements are compared for the best estimate set of flux values, 13 signals with the highest deviations from their respective measurements and contributing 50 % of the error to the Residuum were selected (Table S6, S7). The biggest deviations were observed for m_0 signals, indicating that the effect of dilution of label by unlabeled precursors was not always exactly explained by the model. Possibly a correction for the presence of unlabeled biomass could further improve the fit. If the above 13 measurements were removed from the MS data set and flux parameter fitting started again, the model still consistently converged to the same solution. This means that these measurements are truly redundant and can be removed from the data set without loss of information - and demonstrates the robustness of the model achieved by over-determination.

4.3 Using multiple different labeling experiments improves flux determination in compartmented cells

In plant cells, subcellular compartmentation increases the number of metabolic pools and fluxes connecting these pools, which presents a challenge to reliably estimating the fluxes of central metabolism (Schwender et al., 2004b). The most common approach in ^{13}C-constrained metabolic flux analysis is to use labeled glucose. The information content in the labeled metabolites with respect to flux can be improved by *a priori* design of labeling experiments, resulting in optimized mixtures of different labeled glucose (Mollney et al., 1999). For example a mixture of [1,2-$^{13}C_2$]glucose and [U-$^{13}C_6$]Glucose can be more informative than using [U-$^{13}C_6$]glucose alone. Here we improve the information content of the labeling experiments by combining labeling data from three different labeling experiments ([1,2-$^{13}C_2$]glucose / [U-$^{13}C_6$]glucose, [U-$^{13}C_3$]Ala, and [U-$^{13}C_5$]Gln). If this study had been performed only using a mixture of [1,2-$^{13}C_2$] and [U-$^{13}C_6$]glucose, the resulting standard deviations in several net fluxes would be more than 3 times higher, rendering $vPyr_1$, $vPyr_2$ and vME not well determined. Also, the model with only [1,2-$^{13}C_2$]/[U-$^{13}C_6$]Glucose measurements did not converge consistently to one solution. There were equally good fits with high variation in the flux $vPyr_1$. The effect of combining labeling data is also illustrated in Fig. S6. There is a low sensitivity for $vPyr_1$ in the MS data after labeling with [1,2-$^{13}C_2$]/[U-$^{13}C_6$]Glucose while the labeling with [U-$^{13}C_3$]Ala contributes most to determine this flux (Fig. S6). Other key fluxes are influenced by measurements from all three labeling experiments i.e. they represent overlapping but not identical information (Fig. S6). In *a priori* design of labeling experiments, the information content of labeling experiments with different labeled substrates is compared by using the volume of the confidence ellipsoid, a statistical measure derived from the covariance matrix of the free fluxes (Mollney et al., 1999). By the same approach the information content for the three labeling experiments ([1,2-$^{13}C_2$]/[U-$^{13}C_6$]Glucose, [U-$^{13}C_3$]Ala and [U-$^{13}C_5$]Gln) was calculated separately and with combined data sets. Accordingly, the average radius of the confidence ellipsoid shrinks at least 3 fold if all three data sets are used in fitting.

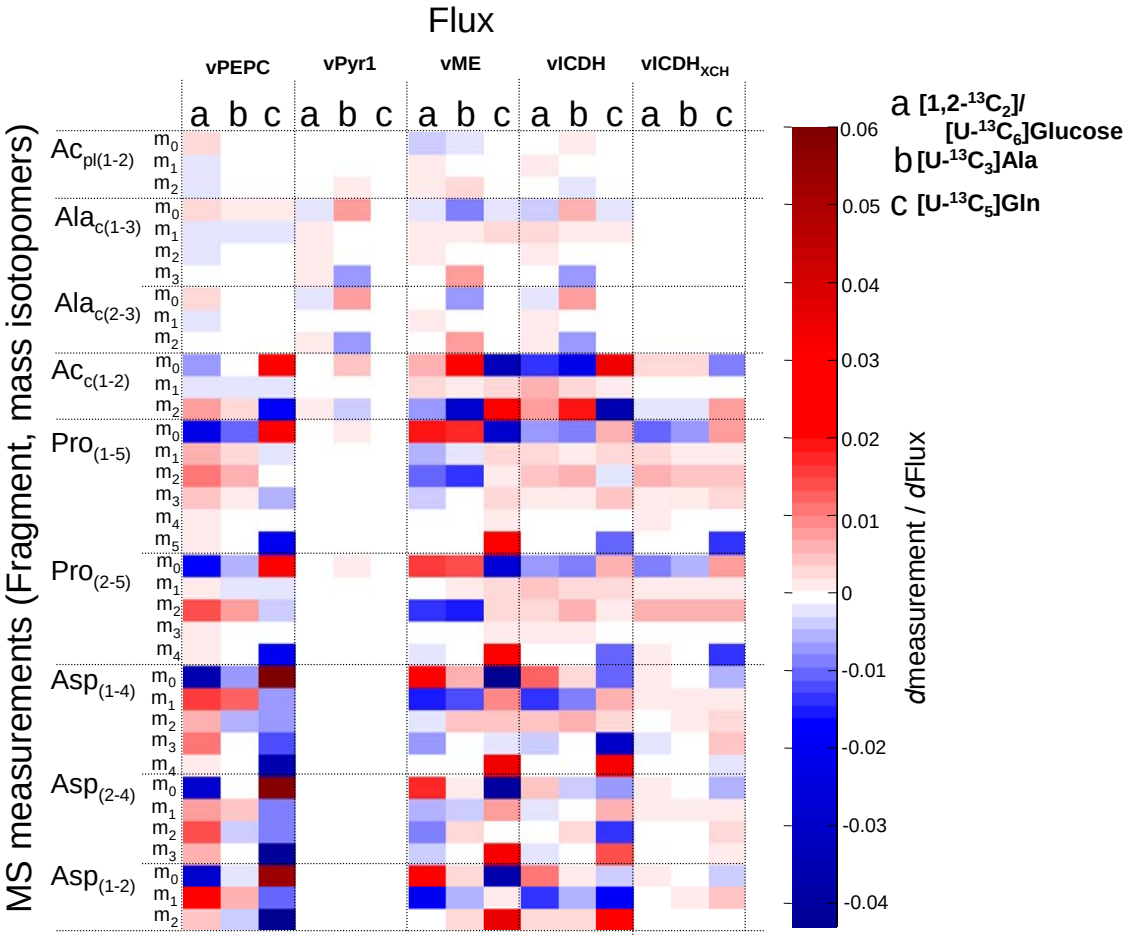

Fig. S6 Increased information content and flux estimate reliability is obtained by combining experiments with different labeled substrates. The sensitivities of several flux values to the MS measurements are shown. Values derived from the output of the isotopomer model (output sensitivity matrix) are shown in color-coded form. Each row refers to an individual mass isotopomer. Each value (*d*measurements/*d*Flux) indicates the change in a predicted mass isotopomer with a very small (differential) change in a free flux (measurements in the scale of fractional enrichment; Flux in nmol h^{-1} mg FW^{-1}). Either dark red or dark blue indicates strong positive or negative correlation between MS measurement and flux as indicated by the scale at the right side. White areas in the figure indicate that these MS measurements do not change with a small change in a particular flux, i.e. these measurements probably do not contain information that helps to define the value of fluxes. The more strong correlations there are, the higher will be the reliability of the flux estimate because redundant measurements exist. One can see that information for the free flux vPyr1 is mainly contained in the experiment with [U-$^{13}C_3$]Ala whereas fluxes for PEPC and ME are best contributed by labeling with [U-$^{13}C_5$]Gln.

5. Statistical Analysis

Normally distributed measurement errors were assumed. With the given best flux estimates and based on the errors in the measurements, the errors in fluxes were calculated via "linearized statistics" (Wiechert et al., 1997) using the *13CFLUX* tool *EstimateStat*. As outlined below, in order to get realistic values for the errors in the fluxes, we considered the uncertainties in the biomass composition (5.1) as well as the errors in the MS measurements that are derived from experimental repetition of the embryo cultures (5.2).

5.1 Error in biomass proportions (Tables S1 – S3).
For fluxes derived from biomass proportions statistical errors were generated by a Monte Carlo approach. Uncertainties in biomass composition were assumed to have a SD of 10% in protein content, oil content and amino acid composition as well as a 10 % uncertainty in the relative abundance of cruciferin, napin and oleosin in storage protein. The statistical variation in the fatty acid composition is taken from Schwender and Ohlrogge (2002). Using these standard deviations random noise was added to the biomass parameters. The random number generator of Microsoft *EXCEL* was used and $N(\mu, \delta)$ distributed numbers were derived according to Box and Müller (1958). Biomass derived fluxes were calculated as described in section 3.1 using the noise added values for biomass composition. The repetition of this procedure 20 times leads to standard deviations in the biomass derived fluxes (Tables S2, S3).

5.2 Error in MS Measurements. In total 164 measurement values derived from GC/MS were considered for flux parameter fitting as well as for the estimation of statistical noise (Fig. S4, Table S6 + S7). Each individual measurement is an average of three GC/MS runs of the same sample. For 90 % of all MS peaks the instrumental SD was < 0.3 % in the fractional enrichment scale. Considering the three ^{13}C-labeling experiments ([1,2-$^{13}C_2$]Glc /[U-$^{13}C_6$]Glc, [U-$^{13}C_5$]Gln, [U-$^{13}C_3$]Ala) the real errors associated with biological repetition should be much larger. In labeling experiments with *B. napus* embryos growing on [U-$^{13}C_6$]glucose and averaging three biological repetitions we observed biological standard errors in MS measurements between about 0 and 2 % (data not shown). Since there are three independent experiments combined in the dataset, the error of biological repetition should be contained in the data, although not as repetitions of each individual mass spectrometric measurement. In the absence of biological repetition for each individual MS measurement we estimated one value as a standard deviation being assigned to all MS measurements in the following way: Under the assumption that the difference between the model-predicted and experimental MS measurements is caused only by standard distributed random noise, the X^2 distribution predicts the expected sum of errors (errors weighted by the standard deviations). Accordingly, on a 90 % confidence level and with 110 degrees of freedom in the system (see Box 1), the weighted sum of errors should be equal or less than 131 ($X^2_{110,\ 90\ \%}$ = 131, see Box 2). This is fulfilled if the SD in the MS measurements are 1.0 % or bigger (scale of fractional enrichment; see equ. 2 in Box 2). This means that according to the presence of random noise in the system a SD of at least 1.0 % is to be expected in the MS

measurements. The estimate of > 1.0 % falls within the range of our reference labeling experiments that showed that the SD in MS measurements are between 0 and 2 %.

Box 1: Degrees of Freedom in the metabolic network:
As shown in Tables S6 and S7, 37 molecule fragments with 164 MS measurements are considered in the flux model. For each molecule fragment the sum of mass isotopomers amounts to 1 (100 %). Therefore, for each fragment one value is always redundant and the 164 measurements are reduced by 37 redundancies. In addition, the lower part of the network is determined by 17 free fluxes. In order to solve the system algebraically an equal number of measurements must be given. Therefore, the number of non-redundant MS measurements minus the 17 free fluxes in the system equals the number of measurements by which the system is over-determined, which amounts to 110 (degrees of freedom). In this calculation we do not consider the biomass derived fluxes since these are not changed in flux parameter fitting and we only want to assess the error in the MS measurements.

Using the 1.0 % estimate for SD in MS measurements, the SDs of the fluxes were derived (table S8; table 1, main text) and all net fluxes appear to be statistically determined (i.e. the error is lower than or in the order of magnitude of the flux value).

Box 2: Estimation of standard deviation for MS measurements.
With 110 degrees of freedom in the system the random error in the measurements can be expected to be equal or lower than 131, based on a 90 % significance level ($X^2_{110,\,90\,\%} = 131$).
If the individual SD associated with *n* measurements could be calculated the error in the system would be:

(1) $\chi^2 = \sum_{i=1}^{n} \frac{e_i^2}{\delta_i^2}$,

with $e_i = x_i - p_i$ (*n* independent measurements, x_i being a particular MS measurement and p_i the model prediction for that measurement; δ_i is the SD in each x_i).

In order to estimate the SD from the residuals (e_i), one global δ is assumed in approximation for all measurements. Accordingly equation (1) changes to:

(2) $\chi^2 = \sum_{i=1}^{n} \frac{e_i^2}{\delta^2} = \frac{1}{\delta^2} \sum_{i=1}^{n} e_i^2$.

Based on equation (2) and knowing that the real error X^2 can be maximally 131 ($\chi_{real}^2 \leq \mathrm{X}^2_{df,90\%}$), the global δ can be estimated according to:

(3) $\delta \geq \sqrt{\frac{1}{\mathrm{X}^2_{df,90\%}} \sum_{i=1}^{n} e_i^2}$

The sum of squared residuals as derived from the data shown in Table S6 and S7 is **0.014**. With $X^2_{110,\,90\,\%} = 131$ the value of δ is estimated to be >= **0.010**.

6. Model Validation

One important prerequisite for the trustworthiness of the flux estimates is that quasi-steady state can be assumed. In addition, the model network can be validated by biochemical data (e.g. subcellular localization of enzymes) and by the labeling data itself. In the following sections, different assumptions that determine the network topology are described and justified.

6.1 Isotopic steady state. Isotopomer balancing under steady state relies on the isotopomer composition of metabolites being constant over time. During culture of the embryos the biomass doubled 4 to 5 times. Therefore at least 95 % of the biomass was formed during culture. The free amino acids are assumed to have a turnover time on the time scale of hours to days. Degradation of proteins and oil was assumed not to contribute significantly to the labeling of central metabolites. The isotopic steady state in free metabolites was assumed to be established after about 3 d of culture while the label in protein-bound amino acids after 14 d should average the label in free amino acids over the entire period of biomass increase. To test isotopic steady state over the labeling period the labeling in protein was compared to the label in free amino acids after 3 d. In the experiment with [U-$^{13}C_6$]Gln the label in protein bound amino acids after 14 d of growth was compared with the label in free amino acids extracted after a 3 d incubation (data not shown). 24 MS signals from 6 fragments were compared (18 degrees of freedom). With an allowed sum of squared differences of $X^2_{18,\,90\,\%} = 26$ the SD had to be 1.6% in the scale of fractional enrichments. Thus with the estimated SD in the system being the same number (see section 5.2) the labeling pattern observed after 3d in free metabolites and after 14 d in protein represented the same labeling pattern. Similar results were obtained with the labeling experiment using [1,2-$^{13}C_2$]/[U-$^{13}C_6$]glucose. The label accumulated in protein and the label in free amino acids after 14d were compared and were also consistent with one another on the basis of a 1.5 % SD.

6.2 Metabolic steady state. In order to maintain a constant concentration of each nutrient in the medium, embryos were cultured in a surplus of culture medium. In the experiments reported we observed biomass increase of about 0.5 mg DW per ml culture medium and according to uptake and biosynthesis rates shown in Fig. 1 (main text) none of the organic substrates in the medium was depleted by more than 10 %. In addition the uptake rates of the different carbon sources remained constant over time. This was concluded from the mass isotopomer distribution in molecular ions of labeled fatty acids according to (Schwender and Ohlrogge, 2002). After feeding [U-$^{13}C_3$]Ala for 14d, the mass isotopomer distribution observed in the molecular ion of C18:0 was in good agreement with the expected pattern due to the condensation of 9 acetate units being uniformly labeled to 7.5 % ^{13}C (data not shown). Significant change in the uptake of [U-$^{13}C_3$]Ala relative to other carbon sources during growth would have resulted in sub-populations of fatty acids labeled differently, with the mass isotopomers in the molecular ion deviating from the expected binominal distribution of a polymer $[acetate]_9$. Similarly, by feeding ^{13}C-labeled glucose, carbon from glucose and sucrose will be mixed at the level of hexose phosphates. As shown before (Schwender and Ohlrogge, 2002) under the culture conditions used here over 90 % of the biomass is formed from a constant mixture

of sucrose and glucose, resulting in constant dilution of the labeled glucose by hexose units derived from sucrose. We conclude that during growth the embryos take up all the different carbon sources in a constant ratio, allowing steady state flux analysis. We also noted that, if the medium concentrations of the organic nutrients are considered, Glc was preferentially taken up compared to Suc and Ala uptake was favored over Gln.

6.3 Isotopic equilibrium of transaminases. As described in section 4.1, based on ^{15}N-Ala labeling the exchange flux between Ala_{cyt} and $pyruvate_{cyt}$ was found to be about 30 times the net flux. In a similar way the ^{13}C-model assigned exchange between Glu_c and KG_m to be more than 10 times the net flux through these pools, indicating isotopic equilibration between the two. For Glu/KG this was independently confirmed from the ^{15}N-labeling experiments. Feeding ^{15}N-Ala (together with $^{14}N_2$-Gln) resulted in a ^{15}N-enrichment of 45 % in the amino-N positions of all protein-bound amino acids, including Pro (data not shown). This isotopic equilibration between ^{15}N and ^{14}N in Pro shows that transaminase activities rapidly interconvert Glu with ketoglutarate.

6.4 Isotopic equilibrium among C4 dicarboxylic acids. The label in protein bound Asp was used in this study to reflect C4-dicarboxylic acids. Cytosolic Asp incorporated into protein is assumed to be derived from cytosolic OAA provided that abundant Asp transaminase activity is present in the cytosol. However, in Asp the labeling signature of symmetric randomization due to interconversion with fumarate was found. If embryos were labeled with [1,2-$^{13}C_2$]glucose / [U-$^{13}C_6$]glucose, central metabolism should generate the isotopomer [1,2,3-$^{13}C_3$]PEP in abundance which, after carboxylation by PEP carboxylase, should produce [1,2,3-$^{13}C_3$]OAA. Without additional reactions, [2,3,4-$^{13}C_3$]OAA is not to be expected. However, the mass isotopomer distribution found in the fragments $Asp_{(1-4)}$, $Asp_{(1-2)}$ and $Asp_{(2-4)}$ shows that there was an almost equal abundance of the isotopomers [1,2,3-$^{13}C_3$] OAA_{cyt} and [2,3,4-$^{13}C_3$]OAA_{cyt}. This symmetric randomization of label in OAA_c can be explained by the symmetry of fumarate if OAA_c and fumarate are rapidly inter-converted. Since in plants fumarase has been found to be confined to mitochondria (Behal & Oliver, 1997), it can be concluded that cytosolic OAA isotopically equilibrates with mitochondrial fumarate by the combination of highly active dicarboxylic acid transporters, malate dehydrogenase and mitochondrial fumarase. Therefore, in the flux model mitochondrial and cytosolic OAA and malate were combined into one metabolic pool and the mitochondrial inter-conversion with fumarate was implemented as a free (*a priori* unknown) exchange flux. The resulting exchange flux was the biggest flux in the system after $vAAT_{XCH}$. Randomization of label in OAA/malate by fumarase has also been observed in maize root tips (Salon et al., 1988; Dieuaide-Noubhani et al., 1995; Edwards et al., 1998), in tomato cell culture (Rontein et al., 2002) and in animal systems (Des Rosiers et al., 1994).

6.5 Isotopic equilibrium of cytosolic and plastidic phosphoenol pyruvate. The only metabolites representing PEP that are accessible in the MS data are the aromatic amino acids. However, these are formed in the plastid and therefore represent plastidic PEP. No labeling information on cytosolic PEP is present and the isotopic equilibration of plastidic and cytosolic pools cannot be directly determined. However, according to Kubis et al. (2004), in isolated plastids of developing *B. napus* embryos at mid-oil stage the capacity

of PEP import matches the *in vivo* rate of fatty acid synthesis. This suggests that the PEP translocator (PPT) is abundant. Therefore we assume isotopic equilibration of PEP_{cyt} and PEP_{pl} by bidirectional exchange between cytoplasm and plastid, and we unify both into one PEP pool in the flux model. This assumption is also supported from the way that PEP is produced. PEP is formed from PGA either in the cytosol or in the plastid (formation of PEP from pyruvate or OAA could be excluded based on labeling experiments, see section 1.1). PGA itself can be rapidly exchanged between cytosol and plastid by the reversible triose phosphate translocator (TPT) which is also abundant in developing seeds of *B. napus* (Gupta and Singh, 1996) and is expressed in abundance in *Arabidopsis* developing seeds (Ruuska et al., 2002). Thus both TPT and PPT will contribute to the isotopic equilibration of the cytosolic and plastidic PEP pools.

6.6 The pyruvate carrier. Uptake kinetics with isolated plastids suggest the presence of a plastidic pyruvate carrier in *B. napus* embryos (Eastmond and Rawsthorne, 2000). As has been shown in the case of the mitochondrial pyruvate carrier (Laloi, 1999), both the mitochondrial and the plastidic pyruvate carrier were assumed to be driven by pH gradients and therefore to work unidirectionally, having essentially no exchange flux. Furthermore, the observed difference in label between (cytosolic) Ala and Val (derived from plastid pyruvate) demonstrates that cytosolic and plastidic pyruvate are not isotopically equilibrated. Therefore, in the flux model the import of pyruvate into the plastids and mitochondria was modeled as non-reversible.

6.7 Independent confirmation of the uptake ratio of Ala and Gln by ^{15}N labeling. Ala and Gln were the sole nitrogen sources in the culture medium. After labeling *B. napus* embryos with (amide) ^{15}N-Gln, (amino) ^{15}N-Gln and ^{15}N-Ala (all 99 % ^{15}N enriched), the ^{15}N enrichment in proteinogenic amino acids was determined by GC/MS. After labeling with ^{15}N-Ala a ^{15}N-enrichment of 45 % was consistently found in the amino-N positions of all amino acids (Data not shown). The results from (amide)-^{15}N-Gln and (amino)-^{15}N-Gln labeling experiments show that 45 % of the protein bound nitrogen positions are derived from Ala and 55 % derived from Gln. Taking into account that Ala and Gln contain one and two nitrogens respectively, the labeling results can be explained by an uptake ratio of Ala:Gln being 62:38 (mol/mol). This ratio was confirmed independently by the ^{13}C-studies, where the influx of Ala and Gln were determined to be in the ratio 63:37 (Fig. 1, main text).

6.8 Influence of atmospheric CO_2. Although there is a net output of CO_2 from the embryo cultures, the influence of unlabeled CO_2 from the atmosphere on the results of labeling experiments has to be considered. We have performed labeling experiments under identical conditions as reported in the paper except that to an unlabeled growth medium ^{13}C-enriched CO_2 (99% ^{13}C enrichment) was given at a 2 % (v/v) concentration in the air space above the medium. We found in all analyzed metabolites a maximum positional enrichment of 12 % ^{13}C. Considering Fick's 1st law of diffusion and a constant CO_2 concentration in the embryos, the diffusion rate of atmospheric CO_2 into the embryos will change in linear correlation to it's concentration in the air. In this case the diffusion rate of CO_2 at ambient 0.037 % in air (370 ppm) would be 57 times less than the diffusion rate of CO_2 concentrated at 2 % (2% / 0.037%). Considering the maximal

12% positional ^{13}C-enrichment in metabolites under 2 % $^{13}CO_2$ in air, this means the fraction of ^{12}C in any C-position in the network derived by air-borne $^{12}CO_2$ would be increased by maximal 0.2 % in the fractional enrichment scale (12% ^{13}C / 57 = 0.2% ^{13}C, or ^{12}C in the case of unlabeled ambient CO_2). Therefore the influence of atmospheric CO_2 on the labeling pattern can be assumed to be insignificant and ignored in isotopomer analysis.

7. Supplemental Tables

	% (w/w) of biomass	SD
TAG	38 %	3.8 %
Total protein	17 %	1.7 %
Cell wall / starch	37 %	3.7 %
other compounds	8 %	

Table S1 Biomass composition of cultured *B. napus* embryos. Main storage compounds in embryos grown under conditions identical to this study. In short, embryos were homogenized and extracted in hexane/isopropanol (2:1) (Lipid extract) and methanol/water (8:2). After transesterification of the lipid fraction, lipid was quantified by gas chromatography of fatty acid methyl esters with glyceryl triheptadecanoate as internal standard. In the remaining cell pellet protein was determined after extraction (1 % sodium dodecyl sulfate, 1 mM β-mercaptoethanol, 50 mM Tris pH 8.0) by BCA assay (Sigma, St. Louis) and confirmed by C/N analysis of dry embryos. The weight of the cell pellet minus protein was assumed to be a glucose polymer with molecular weight of 162 g/mol of the monomers.

	Main seed protein components			
	Cruciferin	Napin	Oleosin	
	(% w/w) 60 ± 6	20 ± 2	20 ± 2	Composition of seed protein (mol %)
Ala	6.7	6.2	7.4	6.7 ± 0.1
Arg	5.7	3.9	8.6	5.7 ± 0.2
Asn	5.9	3.9	0.6	4.6 ± 0.3
Asp	4.0	3.9	8.6	4.7 ± 0.3
Cys	1.0	4.5	0.0	1.6 ± 0.1
Glu	3.8	5.1	1.1	3.7 ± 0.2
Gln	12.3	14.6	6.3	11.8 ± 0.4
Gly	10.7	5.6	10.3	9.6 ± 0.1
His	2.0	1.7	1.1	1.8 ± 0.1
Ile	4.8	2.8	6.3	4.6 ± 0.1
Leu	8.3	7.9	8.6	8.2 ± 0.1
Lys	3.0	5.6	4.6	3.8 ± 0.1
Meth	1.2	2.8	2.9	1.8 ± 0.1
Phe	4.0	5.6	2.3	4.1 ± 0.1
Pro	5.0	7.9	2.9	5.3 ± 0.3
Ser	7.7	5.1	7.4	7.1 ± 0.1
Thr	3.8	5.1	8.6	4.8 ± 0.3
Trp	1.0	1.1	0.6	1.0 ± 0.1
Tyr	2.2	1.7	5.7	2.6 ± 0.2
Val	6.9	5.1	6.3	6.4 ± 0.1

Table S2 Amino acid composition of proteins in *B. napus* embryos. The seed storage protein in *B. napus* consists of 60 % cruciferin, 20 % napin and 20 % oleosin (Norton, 1989). The amino acid compositions of the three proteins were derived from sequence data (NCBI protein database). The amino acid composition of seed protein was calculated considering the amino acid compositions (mol %) of the three protein components and assuming a 10 % SD in the values for the protein fractions. The resulting amino acid composition is similar to the analysis of total seed protein reported by Norton (1989).

Fatty acid compostion		**Biosynthetic precursor demands**		
Fatty acid	Mol %	$Acetate_{pl}$	$Acetate_{cyt}$	glycerol
C16:0	7.4 ± 1.4	24	0	
C18:0	1.9 ± 0.3	27	0	
C18:1	16.2 ± 2.8	27	0	
C18:2	19.6 ± 2.7	27	0	
C18:3	15.3 ± 1.5	27	0	
C20:0	1.0 ± 0.2	27	3	
C20:1	9.1 ± 0.8	27	3	
C22:0	1.0 ± 0.2	27	6	
C22:1	28.6 ± 1.6	27	6	
glycerol	100			1
Total precursor demand per mol TAG		**26.8 ±1.2**	**2.1 ±0.2**	**1**

Table S3 Fatty acid composition of TAG and biosynthetic precursor demands. The fatty acid composition (Mol %) of cultured *B. napus* embryos (cv. Reston) was analyzed by gas chromatography (Data taken from Schwender et al., 2002). Also biosynthetic demands of plastidic and cytosolic acetyl-CoA are given: For each fatty acid species the amount of cytosolic or plastidic acetyl-CoA needed for the synthesis of one molecule triacylglycerol is given. C20 and C22 are derived by cytosolic elongation (cytosolic acetyl-CoA) of C18 fatty acids by one and two units of cytosolic acetyl-CoA, respectively. The SDs of precursor demands are derived from the SD in the fatty acids composition by a Monte Carlo approach.

GC/MS Fragment measured	Metabolic precursor (part of the precursor that contributes)
$Ala_{(1-3)}$	$Pyr_{cyt\ (1-3)}$
$Ala_{(2-3)}$	$Pyr_{cyt\ (2-3)}$
$C18_{(1-2)}$	$AcCoA_{pl\ (1-2)}$
$C22_{(1-2)}$	$AcCoA_{cyt\ (1-2)}$
$Val_{(1-5)}$	$Pyr_{pl\ (1-3)}$ x $Pyr_{pl\ (2-3)}$
$Val_{(2-5)}$	$Pyr_{pl\ (2-3)}$ x $Pyr_{pl\ (2-3)}$
$Pro_{(1-5)}$	$Glu_{cyt\ (1-5)}$
$Pro_{(2-5)}$	$Glu_{cyt\ (2-5)}$
$Asp_{(1-4)}$	$OAA_{cyt\ (1-4)}$
$Asp_{(1-2)}$	$OAA_{cyt\ (1-2)}$
$Asp_{(2-4)}$	$OAA_{cyt\ (2-4)}$

Table S4 Precursor – product relationship according to biosynthetic relations and carbon transitions. Suffixes denote carbon atoms which are referred to. Suffix "cyt" = cytosolic; "pl" = plastidic. See also Fig. S2.

Monomer	precursor from central metabolism												
	$AcCoA_{pl}$	$AcCoA_{cyt}$	Pyr_{pl}	Pyr_{cl}	PEP	OAA_{cyt}	Glu_{cyt}	Gln_{cyt}	CO_2	E4P	PGA	DHAP	PentP
Ala				-1									
Arg							-1		-1				
Asn						-1							
Asp						-1							
Cys											-1		
Glu							-1						
Gln								-1					
Gly									1		-1		
His													-1
Ile			-1			-1			1				
Leu	-1		-2						1				
Lys			-1			-1			1				
Meth						-1					-1		
Phe					-2				1	-1			
Pro							-1						
Ser											-1		
Thr													
Trp			1		-2				1	-1	-1		-1
Tyr					-2				1	-1			
Val			-2						1				
$acetate_{pl}$	-1												
$acetate_{cyt}$		-1											
glycerol												-1	

Table S5 Biosynthetic stoichiometric relations between metabolites of central metabolism and monomers of storage polymers (Protein, TAG). This table is a matrix used to translate the fractions of monomers in biomass (Tables S1, S2) into the biosynthetic demands of intermediate precursors. Information on the pathways can be seen at http://www.arabidopsis.org:1555/ARA/

		Labeled precursors					
		[1,2-$^{13}C_2$]glucose/ [U-$^{13}C_6$]glucose		[U-$^{13}C_3$]Ala		[U-$^{13}C_5$]Gln, 50 %	
Fragment		**Measured**	**Predicted**	**Measured**	**Predicted**	**Measured**	**Predicted**
Ala$_{(1-3)}$	m_0	0.814	0.801	0.675	0.678	0.991	0.998
	m_1	0.046	0.042	0.017	0.013	0.004	0.002
	m_2	0.069	0.078	0.020	0.009	0.002	0.000
	m_3	0.071	0.079	0.289	0.300	0.003	0.000
Ala$_{(2-3)}$	m_0	**0.850**	0.828	0.687	0.690	0.993	1.000
	m_1	0.011	0.019	0.016	0.006	0.002	0.000
	m_2	0.139	0.153	0.297	0.303	0.005	0.000
C18$_{(1-2)}$	m_0	0.761	0.770	0.922	0.924	0.989	1.000
	m_1	0.032	0.025	0.006	0.002	0.004	0.000
	m_2	0.207	0.205	0.072	0.074	0.006	0.000
C22$_{(1-2)}$	m_0	0.879	0.863	**0.878**	0.857	0.844	0.833
	m_1	0.027	0.023	0.010	0.009	0.017	0.010
	m_2	**0.094**	0.115	**0.112**	0.134	**0.139**	0.156
Val$_{(1-5)}$	m_0	**0.541**	0.565	0.834	0.838	0.982	0.997
	m_1	0.065	0.061	0.018	0.018	0.005	0.003
	m_2	0.236	0.233	0.073	0.069	0.009	0.000
	m_3	0.101	0.095	0.069	0.069	0.003	0.000
	m_4	0.028	0.024	-0.001	0.000	0.000	0.000
	m_5	0.029	0.022	0.008	0.005	0.000	0.000
Val$_{(2-5)}$	m_0	**0.564**	0.592	0.842	0.853	**0.981**	1.000
	m_1	0.046	0.038	0.010	0.004	0.007	0.000
	m_2	0.328	0.317	0.140	0.137	0.012	0.000
	m_3	0.007	0.010	-0.001	0.000	0.000	0.000
	m_4	0.055	0.042	0.007	0.006	0.000	0.000
Pro$_{(1-5)}$	m_0	**0.918**	0.890	0.914	0.930	0.590	0.574
	m_1	0.022	0.030	0.015	0.017	0.013	0.008
	m_2	0.044	0.059	0.065	0.049	0.018	0.032
	m_3	0.011	0.014	0.004	0.003	0.020	0.029
	m_4	0.004	0.005	0.000	0.000	0.021	0.018
	m_5	0.002	0.002	0.002	0.000	0.337	0.338
Pro$_{(2-5)}$	m_0	**0.930**	0.906	0.927	0.942	**0.602**	0.576
	m_1	0.014	0.018	0.007	0.008	0.007	0.010
	m_2	0.051	0.068	0.066	0.049	0.045	0.058
	m_3	0.001	0.003	0.000	0.001	0.019	0.015
	m_4	0.004	0.006	0.000	0.000	0.326	0.342
Asp$_{(1-4)}$	m_0	0.705	0.695	0.893	0.889	0.804	0.803
	m_1	0.135	0.141	0.090	0.092	0.029	0.018
	m_2	0.083	0.089	0.012	0.018	0.029	0.030
	m_3	0.065	0.064	0.004	0.000	0.099	0.103
	m_4	0.011	0.011	0.000	0.000	0.041	0.045
Asp$_{(1-2)}$	m_0	0.756	0.758	0.936	0.933	0.807	0.810
	m_1	0.098	0.096	0.056	0.059	0.021	0.022
	m_2	0.106	0.107	0.007	0.009	0.070	0.062
Asp$_{(2-4)}$	m_0	0.040	0.039	0.001	0.000	0.102	0.106
	m_1	0.780	0.778	0.949	0.945	0.821	0.823
	m_2	0.160	0.163	0.043	0.047	0.089	0.081
	m_3	0.060	0.059	0.009	0.008	0.090	0.096

Table S6 GC/MS measurements used for flux analysis. Measured and model predicted labeling in amino acids and fatty acids, labeled in three labeling experiments with differently labeled precursors. Predicted values correspond to the best flux estimates. MS measurements are corrected for natural abundance of ^{13}C and for mass isotope contribution of hetero-atoms and of the derivative side chains. Values are normalized (sum of all peaks of one fragment = 1).

Continuation of Table S6 The instrument related SD for MS measurements average 0.0015 +/- 0.003 while the error in between the three experiments is higher by about an order of magnitude.
Boldface numbers: Largest fitting errors for these measurements. These 13 measurements constitute 50 % of the X^2 sum for of errors.

fragment		measured	predicted
m1RP$_{(1-5)}$	m_0	**0.575**	0.551
	m_1	**0.073**	0.095
	m_2	0.188	0.189
	m_3	0.087	0.084
	m_4	0.042	0.043
	m_5	0.034	0.039
m1TP$_{(1-3)}$	m_0	0.710	0.725
	m_1	0.050	0.042
	m_2	0.112	0.107
	m_3	0.128	0.126
m1HP$_{(1-6)}$	m_0	0.578	0.588
	m_1	0.043	0.039
	m_2	0.169	0.175
	m_3	0.073	0.076
	m_4	0.032	0.029
	m_5	0.021	0.017
	m_6	0.083	0.076
m1Gln$_{(1-5)}$	m_0	0.975	0.975
	m_1	0.004	0.007
	m_2	0.014	0.014
	m_3	0.004	0.003
	m_4	0.001	0.001
	m_5	0.002	0.000

Table S7 Measurements considered for the label experiment [1,2-$^{13}C_2$]glucose/ [U-$^{13}C_6$]glucose in addition to the data shown in table S6. The fragment m1Gln$_{(1-5)}$ is derived from a measurement of free Gln.

Metabolites analyzed	**Labeled Precursors**		
	^{15}N-Ala*	[1-^{15}N]-Gln	[5-^{15}N]-Gln
Ala	44.2 ± 0.4 %	31.9 %	17.4 %
Val, Phe, Gly, Ser, Pro	42.1 ± 0.5 %	33.5± 0.2 %	18.1± 0.1 %

Table S7a Average ^{15}N enrichment in different amino acids after feeding differently ^{15}N-labeled Ala and Gln under the same conditions as in the ^{13}C-labeling experiments. Ala or Gln in the medium were enriched to 99 % ^{15}N in the 1– or 5-position. *n = 3 experiments.

Flux name	NET flux	SD	Exchange flux	68 % conficence interval	
				lower bound	upper bound
vuptGlc	58.3	4.2 (4.5*)			
vG6PDH	5.6	2.3 (3.3)			
vRub	19.3	3.5 (4.7)			
Valdo	31.6	3.6 (3.9)	43.8	35.8	52.4
vGAPDH	46.2	7.9 (10.6)	65.4	6.5	185.8
vPGM	83.0	8.3 (8.7)			
vuptAla	7.4	0.7 (2.1)			
vuptGln	4.3	0.3 (0.5)			
vPKc	17.9	2.0 (5.1)			
vPKp	60.0	6.5 (9.3)			
vAAT	6.6	0.7 (2.1)	190.0	106	274
vGlnGlu	3.0	0.2 (0.4)	1.3	0.7	1.8
vPEPC	3.6	0.3 (1.0)			
vME	2.3	0.3 (1.3)			
vCS	5.8	0.6 (0.7)			
vACL	5.9	0.6 (0.7)			
vICDH	-0.1	0.2 (0.4)	4.5	3.5	5.4
vKDH	1.3	0.2 (0.5)			
vFM	1.3	0.2 (0.5)	29.5	13.6	46.9
vGAT	1.4	0.2 (0.4)	4.7	3.6	5.8
$vPyr_1$	21.0	2.6 (7.0)			
$vPyr_2$	3.5	0.3 (1.3)			
vPDH	77.0	8.9 (9.1)			
vCO2_out	71.0	8.7 (10.6)			
vFASt	82.0	8.9 (9.0)			
$vFAS_{pl}$	76.1	8.9 (9.1)			
$vFAS_c$	5.9	0.6 (0.7)			
vAla_P	0.7	0.1 (0.1)			
$vPyr_{pl}$_P	4.0	0.6 (0.6)			
vPEP_P	1.6	0.2 (0.2)			
$vAcCoA_{pl}$_P	0.9	0.1 (0.1)			
vAsp_P	2.6	0.3 (0.4)			
vGlu_P	1.6	0.2 (0.2)			
vGln_P	1.3	0.2 (0.2)			
vHis_P	0.3	0.0 (0.0)			
vEP_P	0.8	0.1 (0.1)			
vSer_P	2.0	0.3 (0.3)			
vGlyc_TAG	2.8	0.3 (0.3)			
vHP_St	15.9	1.4 (1.4)			

Table S8 Best Fit **flux estimates.** This set of flux values [nmol h^{-1} mg FW^{-1}] was obtained consistently by starting the flux parameter fitting with random start values over a hundred times. SD in fluxes are given for a SD of 1.0 % in the MS measurements. For exchange fluxes upper and lower bounds of the unsymmetrical 68 % confidence intervals are given.

* In parentheses are the SD values obtained if only the MS data from the labeling with [1,2-$^{13}C_2$]glucose/ [U-$^{13}C_6$]glucose are considered.

Flux name	Reaction	Enzyme	Net flux	NADH	FADH	ATP
Mitochondrial ATP production by substrate oxidation						
vME	malate → Pyr_{mit} + NADH	Mitochondrial malic enzyme	2..3	2.3		7.0
vCS	OAA + $AcCoA_{mit}$ → Cit	Citrate synthase	5.8			0.0
$vPDH_{mit}$	Pyr_{mit} → $AcCoA_{mit}$ + CO_2 + NADH	Plastidic pyruvate dehydrogenase complex	5.8	5.8		17.5
vICDH	Cit → KG + CO_2 + NADH	Aconitase, Isocitrate dehydrogenase	-0.1	-0.1		-0.2
vKGDH	KG → Succ + CO_2 + NADH + GTP	Ketoglutarate dehydrogenase Succinyl-CoA synthethase	1.3	1.3		4.0
	Succ → Fum + FADH	Succinate dehydrogenase	1.3		1.3	2.6
vFM	Fum → mal	fumarase				
	Mal → OAA + NADH	malate dehydrogenase	1.3	1.3		4.0
ATP produced in mitochondria by oxidative phosphorylation from mitochondrial NADH and FADH[*1]						**34.8**
ATP need for Fatty acid and Protein Synthesis						
$vFAS_{pl}$	$AcCoA_{pl}$ → FA	Plastidic fatty acid synthesis to C16 and C18 fatty acids	76.1			76.1
$vFAS_c$	$AcCoA_{cyt}$ + FA → VLCFA	Cytosolic elongation of C18 fatty acids to C_{20} and C_{22}	5.9			5.9
vACL	Cit → $AcCoA_{cyt}$ +OAA	Cytosolic ATP:Citrate lyase	5.9			5.9
			ATP needed for fatty acid synthesis			**87.9**
		amino acids into protein[*2]	16.6			
			X 4.3 mole ATP / mol AA[*3]			**71.3**
			Total ATP need for protein and TAG synthesis			**159.2**

Table S9. **Estimation of ATP production by mitochondria and ATP demand by biosynthesis of protein and TAG.** Flux values (nmol h^{-1} $mgFW^{-1}$) for *B. napus* embryos taken from table S8. Cofactor balances are given according to fluxes.

*1 maximal possible ATP/O ratios were assumed as 3.0 for NADH and 2.0 for FADH

*2 sum of fluxes into biomass for all amino acids, see Table S2.

*3 estimated cost for protein synthesis was assumed as 4.3 moles ATP per mole amino acid incorporated (Stefanopoulos *et al.*, 1998)

Table S10 Network definition, extract from the model file used in *13CFLUX*. The first sub-network is shown, simulating labeled glucose.

NETWORK

	FLUX_NAME	**EDUCT_1**	**EDUCT_2**	**PRODUCT_1**	**PRODUCT_2**	
// Uptake of substrates						
	vuptU	m1GLCU		m1GLC		//uptake labeled glucose
		#ABCDEF		#ABCDEF		
	vupt0	m1GLC0		m1GLC		//uptake unlabeled glucose
		#ABCDEF		#ABCDEF		
	vupt	m1GLC		m1HP		
		#ABCDEF		#ABCDEF		
	vuptAla	m1Ala_in		m1AlaCyt		//uptake alanine
		#ABC		#ABC		
	vuptGln	m1Gln_in		m1Gln		//uptake glutamine
		#ABCDE		#ABCDE		
// calvin cycle / ppp						
	vG6PDH	m1HP		m1CO2	m1RuP	
		#ABCDEF		#A	#BCDEF	
	vTK1	m1XP	m1RP	m1SP	m1TP	// transketolase
		#ABCDE	#abcde	#ABabcde	#CDE	
	vSaldo	m1SP		m1EP	m1TP	// SHP2 aldolase, reversible
		#ABCDEFG		#DEFG	#CBA	// with Sh bisphosphatase
	vTK2	m1XP	m1EP	m1TP	m1HP	// transketolase
		#ABCDE	#abcd	#CDE	#ABabcd	
	vPPiso	m1RuP		m1RP		// Ru5P epimerase
		#ABCDE		#ABCDE		
	vPPepi	m1RuP		m1XP		// Ru5P isomerase
		#ABCDE		#ABCDE		
	vRub	m1RuP	m1CO2	m1PGA	m1PGA	// RubisCO
		#ABCDE	#a	#aBA	#CDE	

Continuation of table S10

// Embden Meyerhof Pathway						
	valdo	m1HP		m1TP	m1TP	// F1,6P2 aldolase
		#ABCDEF		#CBA	#DEF	
	vGAPDH	m1TP		m1PGA		// GAP-dehydrogenase
		#ABC		#ABC		
	vPGM	m1PGA		m1PEP		// P-glycerate mutase, enolase
		#ABC		#ABC		
	vAAT	m1AlaCyt		m1PyrCyt		// Ala / XXX transaminase
		#ABC		#ABC		
// cytosolic and plastidic metabolism of PEP, Pyruvate, Ala, Glu						
	vPKc	m1PEP		m1PyrCyt		// cytosolic pyruvate kinase
		#ABC		#ABC		// compartmentation of PEP is not considered
	vPKpl	m1PEP		m1PyrPl		// plastidic pyruvate kinase
		#ABC		#ABC		
	vPEPC	m1PEP	m1CO2	m1OAA		// PEP carboxylase
		#ABC	#a	#ABCa		
	vGlnGlu	m1Gln		m1Glu		// Glutaminase
		#ABCDE		#ABCDE		// glutamate synthase
	vGAT	m1Glu		m1KG		// glutamate/KG transaminase
		#ABCDE		#ABCDE		// and exchange cytosol / mitochondrium
	vPyr1	m1PyrCyt		m1PyrPl		// pyruvate import into plastid
		#ABC		#ABC		
	vPyr2	m1PyrCyt		m1Pyrm		// Import of pyruvate into mitochondria
		#ABC		#ABC		
	vVal	m1PyrPl	m1PyrPl	m1Val	m1CO2	// plastidic valine synthesis
		#ABC	#abc	#ABbcC	#a	
	vPDHpl	m1PyrPl		m1AcPl	m1CO2	// formation of plastidic acetyl-CoA
		#abc		#bc	#a	// major CO2 producer
	vFASPl	m1AcPl		m1AcFA		// plastidic fatty acid synthesis
		#AB		#AB		// AcFA is also fueled from AcCyt
	vAco	m1Cit		m1Icit		// Aconitate hydratase
		#ABCDEF		#EDCBAF		

Continuation of table S10

	vACL	m1Cit #ABCDEF	m1OAA #FCDE	m1AcCyt #AB	// ATP:citrate lyase
	vICDH	m1Icit #ABCDEF	m1KG #ABCDE	m1CO2 #F	// isocitrate dehydrogenase
	vKDHa	m1KG #ABCDE	m1Succ #BCDE	m1CO2 #A	// ketoglutarate dehydrogenase
	vKDHb	m1KG #ABCDE	m1Succ #EDCB	m1CO2 #A	// two reactions for symmetric // randomization in succinate
	vFM1	m1Succ #ABCD	m1OAA #ABCD		// Fumarase, malate dehydrogenase
	vFM2	m1Succ #ABCD	m1OAA #DCBA		// two reactions for symmetric // randomization in succinate
	vME	m1OAA #ABCD	m1Pyrm #ABC	m1CO2 #D	// mitochondrial malic enzyme
	vFAScyt	m1AcCyt #AB	m1AcFA #AB		// cytosolic fatty acid elongation // AcFA is also fueled from AcPl
// output					
	vCO2_out	m1CO2 #A	m1CO2_out #A		// CO2 release
	vAla_P	m1AlaCyt #ABC	m1AlaP #ABC		// Ala into protein
	vPyrpl_P	m1Val #ABCDE	m1ValP #ABCDE		// Val into protein // also Leu, Ile, Lys
	vAsp_P	m1OAA #ABCD	m1Asp #ABCD		// Asp into protein // also Asn, Thr, Met, Ile, Lys
	vGlu_P	m1Glu #ABCDE	m1Gluprot #ABCDE		// Glu into protein // also Pro, Arg
	vGln_P	m1Gln #ABCDE	m1Glnprot #ABCDE		// Gln into protein
	vFAS	m1AcFA #AB	m1AcFA_out #AB		// Acetate units into fatty acids // plastidic FA synthesis + cytosolic elongation
	vPEP_P	m1PEP #ABC	m1PEP_P #ABC		// PEP into Phe, Tyr, Trp (protein)

Continuation of table S10

vAcpl_P	m1AcPl #AB	m1Ac_P #AB	// Acpl into Leu (protein)
vHis_P	m1RP #ABCDE	m1PrPP #ABCDE	// RP into His, Trp
vEP_P	m1EP #ABCD	m1Aro #ABCD	// E4P into aromatic AA
vSer_P	m1PGA #ABC	m1Ser #ABC	// PGA into Ser, Gly, Cys
vGlyc_TAG	m1TP #ABC	m1glycerol #ABC	// glycerol part of TAG
vHP_St	m1HP #ABCDEF	m1St #ABCDEF	// HP into starch and cell wall polymers

8. References

Box, G.E.P., and Müller, M.E. (1958) A note on the generation of random normal deviates. *Annals Math. Stat* **29**, 610-611

Behal, R.H., and Oliver, D.J. (1997) Biochemical and molecular characterization of fumarase from plants: Purification and characterization of the enzyme—cloning, sequencing, and expression of the gene. *Arch Biochem Biophys* **348**, 65–74

Chia, T.Y.P., Pike, M.J., and Rawsthorne, S. (2005) Storage oil breakdown during embryo development of *Brassica napus* (L.). *J. Exp. Bot.* **56**, 1285-1296

Dennis, D. T. (1989) in Physiology, Biochemistry, and Genetics of Nongreen Plastids (Boyer, C. D., Shannon, R. C., and Hardison, R. C., eds) pp. 120–129, American Society of Plant Physiologists, Rockville, MD

Des Rosiers, C., Fernandez, C.A., David, F., and Brunengraber, H. (1994) Reversibility of the mitochondrial isocitrate dehydrogenase reaction in the perfused rat liver. Evidence from isotopomer analysis of citric acid cycle intermediates. *J. Biol. Chem.* **269**, 27179-27182

Dieuaide-Noubhani, M., Raffard, G., Canioni, P., Pradet, A., and Raymond, P. (1995) Quantification of compartmented metabolic fluxes in maize root- tips using isotope distribution from C-13-labeled or C-14- labeled glucose. *J. Biol. Chem.* **270**, 13147-13159

Domergue, F., Cassagne, C., and Lessire, R. (1999) Seed acyl-coa elongases: the other system of fatty acid synthesis. Ocl-Ol. *Corps Gras Lipides* 6, 101–106

Eastmond, P. J., and Rawsthorne, S. (2000)Coordinate changes in carbon partitioning and plastidial metabolism during the development of oilseed rape embryo. *Plant Physiol.* **122**, 767-774

Edwards, S., Nguyen, B. T., Do, B., and Roberts, J. K. M. (1998) Contribution of malic enzyme, pyruvate kinase, phosphoenolpyruvate carboxylase, and the Krebs cycle to respiration and biosynthesis and to intracellular ph regulation during hypoxia in maize root tips observed by nuclear magnetic resonance imaging and gas chromatography-mass spectrometry. *Plant Physiol.* **116**, 1073-1081

Goffman, F. D., Ruckle, M., Ohlrogge, J. B., and Shachar-Hill, Y. (2004) Carbon dioxide concentrations are very high in developing oil seeds. *Plant Physiol. Biochem.* **42**, 703-708

Goffman, F.D., Alonso, A.P., Schwender, J., Shachar-Hill, Y., and Ohlrogge, J.B. (2005) Light enables a very high efficiency of carbon storage in developing embryos of rapeseed. *Plant Physiol.* **138**, 2269-2279

Gupta, R., and Singh, R. (1996) Fatty acid synthesis by isolated leucoplasts from developing *Brassica* seeds: role of nucleoside triphosphates and DHAP- shuttle as the source of energy. *J. Biosciences* **21**, 819-826

Ireland, R. J., and Lea, J. P. (1999) in Plant Amino Acids: Biochemistry and Biotechnology (Singh, B. K., ed.) pp. 49–109, Marcel Dekker, New York

Kubis, S.E., Pike, M.J., Everett, C.J., Hill, L.M., and Rawsthorne, S. (2004) The import of phosphoenolpyruvate by plastids from developing embryos of oilseed rape, *Brassica*

napus (L.), and its potential as a substrate for fatty acid synthesis. *J. Exp. Bot.* **55**, 1455–1462

Ho, C. L., Noij, M., and Saito, K. (1999) Plastidic pathway of serine biosynthesis. *J. Biol. Chem.* **274**, 11007–11012

Laloi, M. (1999) Plant mitochondrial carriers: an overview. *Cell. Mol. Life Sci.* **56**, 918–944

Mollney, M., Wiechert, W., Kownatzki, D., and de Graaf, A.A. (1999) Bidirectional reaction steps in metabolic networks part IV: Optimal design of isotopomer labeling experiments. *Biotechnol. Bioeng.* **66**, 86–103

Norton, G. Nature and biosynthesis of storage proteins. In G Röbbelen, RK Downey, A Ashri, eds., Oil Crops of the World. McGraw Hill, NY, pp 165-191 (1989)

Ohta, D., Fujimori, K., Mizutani, M., Nakayama, Y., Kunpaisal-Hashimoto, R., Münzer, S., and Kozaki, A. (2000) Molecular cloning and characterization of ATP-phosphoribosyl transferase from *Arabidopsis*, a key enzyme in the histidine biosynthetic pathway. *Plant Physiol.* **122**, 907–914

Ruuska, S., Girke, T., Benning, C., and Ohlrogge, J.B. (2002) Contrapuntal networks of gene expression during *Arabidopsis* seed filling. *Plant Cell* **14**, 1191-1206

Ruuska, A.S., Schwender, J., and Ohlrogge, J.B. (2004) The capacity of green oilseeds to utilize photosynthesis to drive biosynthetic processes. *Plant Physiol.* **136**, 2700-2709

Rontein, D., Dieuaide-Noubhani, M., Dufourc, E. J., Raymond, P., and Rolin, D. (2002) The metabolic architecture of plant cells. Stability of central carbon metabolism and flexibility of anabolic pathways during the growth cycle of tomato cells. *J. Biol. Chem.* **46**, 43948-43960

Salon, C., Raymond, P., and Pradet, A. (1988) Quantification of carbon fluxes through the tricarboxylic acid cycle in early germinating lettuce embryos. *J. Biol. Chem.* **263**, 12278-12287

Schultz, C. J., and Coruzzi, G. M. (1995) The aspartate aminotransferase gene family of *Arabidopsis* encodes isoenzymes localized to three distinct subcellular compartments. *Plant J.* **7**, 61–75

Schwender, J. and Ohlrogge, J.B. (2002) Probing *in vivo* metabolism by stable isotope labeling of storage lipids and proteins in developing *Brassica napus* embryos. *Plant Physiol.* **130**, 347-361

Schwender, J., Ohlrogge, J.B. and Shachar-Hill, Y. (2003) A flux model of glycolysis and the oxidative pentosephosphate pathway in developing *Brassica napus* embryos. *J. Biol. Chem.* **278**, 29442-29453

Schwender, J., Goffman, F., Ohlrogge, J.B. and Shachar-Hill, Y. (2004) RuBisCO without the Calvin cycle improves the carbon efficiency of developing green seeds. *Nature* **432**, 779-782

Schwender, J., Ohlrogge, J. and Shachar-Hill Y (2004b) Understanding flux in plant metabolic networks. *Current Opinion Plant Biol.* **7**, 309-317

Singh, B. K. (1999) in Plant Amino Acids: Biochemistry and Biotechnology (Singh, B. K., ed) pp. 227–247, Marcel Dekker, New York

Stefanopoulos, G. N., Aristidou, A. A. and Nielsen, J. (1998) Metabolic Engineering: Principles and Methodologies, Academic Press, London

Szyperski T (1998) C-13-NMR, MS and metabolic flux balancing in biotechnology research. *Q. Rev. Biophys.* **31**, 41–106

Wiechert, W. and de Graaf, A. (1997) Bidirectional reaction steps in metabolic networks: I. Modeling and simulation of carbon isotope labeling experiments. *Biotechnol. Bioeng.* **55**, 101–117

Wiechert, W., Mollney, M., Isermann, N., Wurzel, M. and de Graaf, A.A. (1999) Bidirectional reaction steps in metabolic networks: III. Explicit solution and analysis of isotopomer labeling systems. *Biotechnol. Bioeng.* **66**, 69-85

Wiechert, W., Siefke, C., de Graaf, A.A. and Marx, A (1997) Metabolic Networks: II. Flux estimation and statistical analysis. *Biotechnol. Bioeng.* **55**, 118–135

Wiechert, W., Mollney, M., Petersen, S. and de Graf, A.A. (2001) A universal framework for ^{13}C metabolic flux analysis. *Metabol. Eng.* **3**, 265-283

Wilkie, S. E. and Warren, M. J. (1998) Recombinant expression, purification, and characterization of three isoenzymes of aspartate aminotransferase from *Arabidopsis thaliana*. *Protein Expression Purif.* **12**, 381–389

Whitfield, H. V., Murphy, D. J., and Hills, M. J. (1993) Subcellular-localization of fatty-acid elongase in developing seeds of *Lunaria annua* and *Brassica napus*. *Phytochemistry* **32**, 255–258